ACS NANO

www.acsnano.org

ARTICLE

Regulating Chemisorption and Electrosorption Activity for Efficient Uptake of Rare Earth Elements in Low Concentration on Oxygen-Doped Molybdenum Disulfide

Weiquan Zhan, Xuan Zhang, Yuan Yuan, Qizheng Weng, Shaoxian Song,* María de Jesús Martínez-López, José Luis Arauz-Lara, and Feifei Jia*

Cite This: *ACS Nano* 2024, 18, 7298–7310

Read Online

ACCESS | Metrics & More | Article Recommendations | Supporting Information

ABSTRACT: Recovery of rare earth elements (REEs) with trace amount in environmental applications and nuclear energy is becoming an increasingly urgent issue due to their genotoxicity and important role in society. Here, highly efficient recovery of low-concentration REEs from aqueous solutions by an enhanced chemisorption and electrosorption process of oxygen-doped molybdenum disulfide (O-doped MoS_2) electrodes is performed. All REEs could be extremely recovered through a chemisorption and electrosorption coupling (CEC) method, and sorption behaviors were related with their outer-shell electrons. Light, medium, and heavy ((La(III), Gd(III), and Y(III)) rare earth elements were chosen for further investigating the adsorption and recovery performances under low-concentration conditions. Recovery of REEs could approach 100% under a low initial concentration condition where different recovery behaviors occurred with variable chemisorption interactions between REEs and O-doped MoS_2. Experimental and theoretical results proved that doping O in MoS_2 not only reduced the transfer resistance and improved the electrical double layer thickness of ion storage but also enhanced the chemical interaction of REEs and MoS_2. Various outer-shell electrons of REEs performed different surficial chemisorption interactions with exposed sulfur and oxygen atoms of O-doped MoS_2. Effects of variants including environmental conditions and operating parameters, such as applied voltage, initial concentration, pH condition, and electrode distance on adsorption capacity and recovery of REEs were examined to optimize the recovery process in order to achieve an ideal selective recovery of REEs. The total desorption of REEs from the O-doped MoS_2 electrode was realized within 120 min while the electrode demonstrated a good cycling performance. This work presented a prospective way in establishing a CEC process with a two-dimensional metal sulfide electrode through structure engineering for efficient recovery of REEs within a low concentration range.

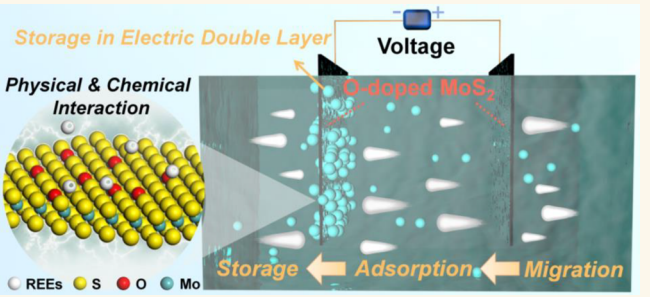

KEYWORDS: *Rare earth element recovery, Low concentration, Chemisorption and electrosorption, Electrical double layer, O-doped MoS_2 electrode*

INTRODUCTION

Due to increasing demands in batteries,[1,2] electronics,[3] the nuclear industry,[4] and other vital fields,[5] rare earth elements (REEs) have been widely applied because of their distinctive physical and chemical properties.[6] Primary and secondary resources, likes ores,[7] manufacturing generated waste,[8,9] and materials based on REEs[10,11] are important resources for REEs. However, generated wastes and effluents during the extraction process from most resources with a low level of REEs will seriously contaminate the ecological environment and cause damage to human health owing to their carcinogenicity and genotoxicity.[12,13] Therefore, there is an urgent need to recover REEs in a low concentration range from aqueous solutions.

Until now, the main methods for separating and/or recovering REEs from aqueous solutions have been chemical

Received: January 16, 2024
Revised: February 13, 2024
Accepted: February 16, 2024
Published: February 20, 2024

https://doi.org/10.1021/acsnano.4c00691
ACS Nano 2024, 18, 7298–7310

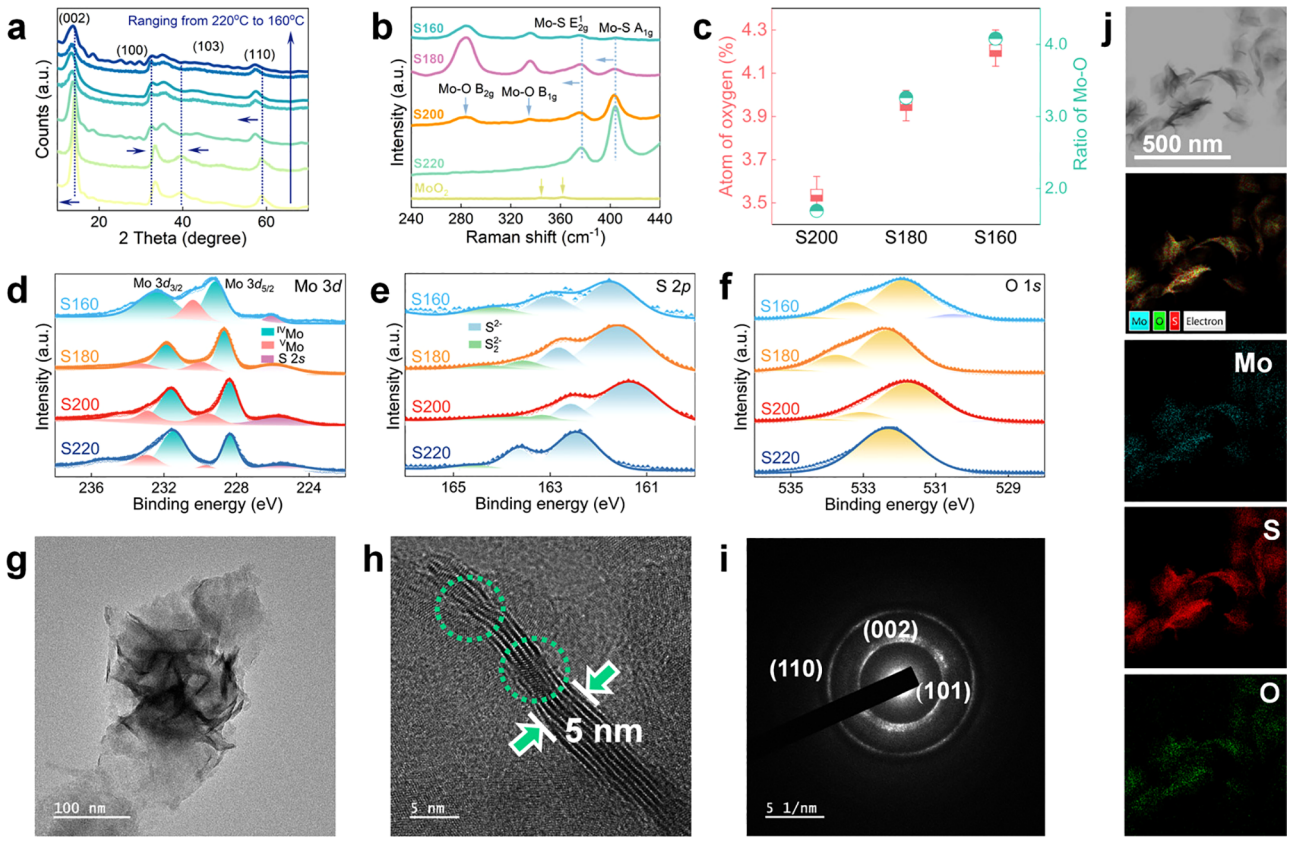

Figure 1. (a) XRD spectra, (b) Raman patterns, (c) oxygen content and ratio of Mo−O bonds, and deconvoluted high-resolution XPS spectra of (d) Mo 3d, (e) S 2p, and (f) O 1s of samples obtained at various synthesis temperatures. (g) TEM image, (h) HRTEM image, (i) SAED pattern, and (j) TEM image and corresponding elemental mapping of O-doped MoS_2.

precipitation,[14,15] ion exchange,[16,17] solvent extraction,[18−20] crystallization,[21−23] and sorption.[24−26] Although various methods have been used for recovering REEs, these conventional methods present several disadvantages like extreme temperature requirements or high consumption of chemicals. Among these strategies, sorption has been widely researched thanks to its economics and environmental friendliness, as well as effective properties. Plenty of materials including activated carbon,[27,28] natural materials functionalized with reactive groups,[29,30] algal resources,[31] minerals,[32,33] cryogels,[34,35] and modified resin microparticles[26] have been adopted to recover REEs including lanthanum (La), yttrium (Y), gadolinium (Gd), neodymium (Nd), terbium (Tb), etc. Nevertheless, the recovery of REEs is far from the full potential in low concentration because of the lack of incentives and technological constraints. Thus, it is of great necessity to explore an efficient method to recover REEs for sustainable development of the environment.

Electrosorption combining an adsorbate with electrochemistry in a system occurs with the application of electricity during the adsorption process.[36−38] In the electrolytic cell, a potentiostat works as a current and voltage resource, and two or more electrodes are connected to an external circuit.[39] The target ions will be first induced for immigration and then overcome the electrostatic repulsion between electrodes and mobile ions in the external electric field.[40] The surface of the material coated on the working electrode reacts with only one type of the components in the electrolyte. Therefore, the interaction between electrolyte and electrode is a chemisorption and electrosorption coupling (CEC) process, which is beneficial for the removal or recovery of targeted ions from solutions.

The CEC process strongly relies on materials with surficial properties for efficient adsorption, and it can realize highly recovery and selectivity with specific ions. It was proved to have a great potential application advantage in heavy metal ions[41−43] like Cr^{3+}, Cd^{2+}, Pb^{2+}, Ni^{2+}, Co^{2+}, Cu^{2+}, and Fe^{3+}. Benefiting from its rich sulfur atoms in the structure, molybdenum disulfide (MoS_2)[44−48] has long been recognized as an outperformer in the sorption of acid metal ions based on the theory of hard and soft acids and bases such as Hg^{2+}, Pb^{2+}, Cu^{2+}, Zn^{2+}, etc. Motivated by the electric performance of MoS_2 as electrode as well as its earth abundance and nontoxicity, it is timely to investigate whether it could be used as an electrode in the recovery of REEs from aqueous solutions.

Due to the relevance of electrochemistry performance of an electrode and its intrinsic conductivity, heteroatom doping has emerged as a powerful tool to tune its electronic properties.[49,50] The heteroatom doping strategies have been widely applied in various fields[51−54] including the hydrogen evolution reaction, capacitive deionization, batteries, etc. It is reported that charge transfer from incorporated atoms could modify the electrical order, like charge density and conductivity. The replacement of S atoms with O atoms would enhance the interface characteristics in the application.[55−57] Consequently, great efforts should be devoted to the understanding of electrochemistry performance of electrodes under the recovery of REEs in low concentration from aqueous solutions.

Herein, we explored the recovery of REEs, especially La(III), Gd(III), and Y(III), as representative REEs, ina low

https://doi.org/10.1021/acsnano.4c00691
ACS Nano 2024, 18, 7298−7310

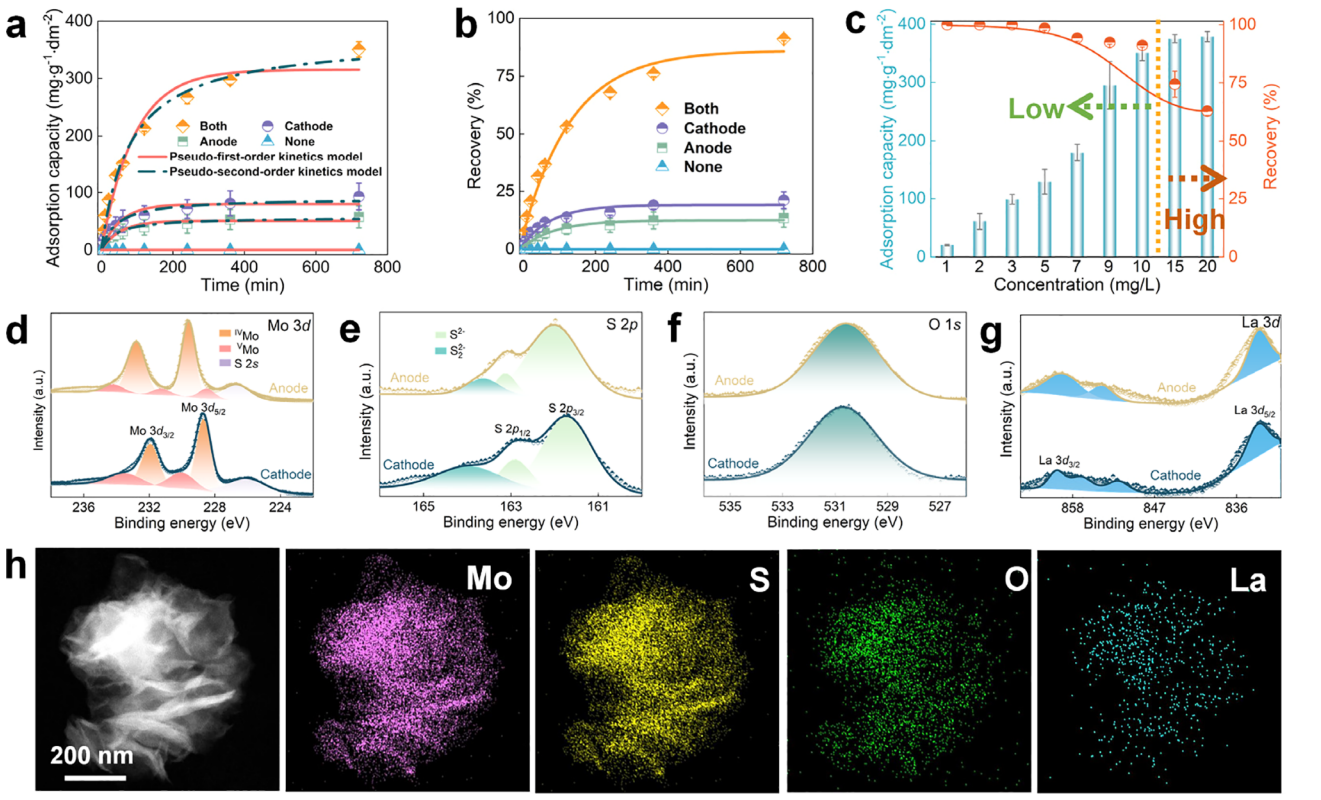

Figure 2. (a) Adsorption capacity and (b) recovery of La(III) on O-doped MoS_2 at an initial concentration of 10 mg/L. (c) Recovery of La(III) at various initial concentrations. High-resolution XPS spectra of (d) Mo 3d, (e) S 2p, (f) O 1s, and (g) La 3d after the recovery of La(III). (h) TEM image and related elemental mapping: Mo, S, O, and La of O-doped MoS_2 after the recovery of La(III).

concentration range from aqueous solutions. Besides, more insights were provided in the aforementioned issues on MoS_2 as electrodes for the adsorption of targeted ions. The fact that MoS_2 with an S−Mo−S lamellar structure belonging to a typical transition metal sulfide not only enables interaction with REEs by rich S atoms but also permits the modulation of chemical and electrical properties through facile heteroatom doping. Considering the strong hydration of REEs, O atoms were introduced into the structure of MoS_2 to improve hydrophilicity, interaction ability, and electrical properties. We further applied a voltage on an MoS_2 electrode to induce immigration of REEs and overcome electrostatic repulsion between surface and target ions in an external electric field. The experimental studies on the CEC process via O-doped MoS_2 electrode showed efficient REE recovery performance, consistent with our theoretical prediction. REE recovery through a CEC process via an O-doped MoS_2 electrode revealed in this study deepens our understanding of the interaction, immigration, and recovery mechanism of REEs on transition-metal sulfides and helps to guide a thought for recovering REEs in a low concentration range for green and recyclable uses.

RESULTS AND DISCUSSION

Structural and Compositional Analysis. The crystalline structure of obtained samples at various synthesis temperatures (220, 210, 200, 190, 180, 170, and 160 °C) was characterized via XRD (Figure 1a), in order to investigate the influence of the synthesis temperature on structure of MoS_2 and the possibility of oxygen doping. Typical peaks located at around 14, 33, 39, and 59° were ascribed to diffractions of (002), (100), (103), and (110) planes[58] of 2H-MoS_2 (JCPDS 37-1492), respectively. Compared with the XRD result of MoO_2 (Figure S1), no peaks for MoO_2 appeared, indicating the absence of MoO_2. The lower synthesis temperature broadened and shifted all the peaks to lower angle compared with the synthesis temperature of 220 °C, indicating the decrease of crystallinity.[59] The inferior crystallinity of MoS_2 might lead to doping of oxygen atoms into the structure. The bond structure of synthesized samples was determined by Raman spectra (Figure 1b), where two dominant peaks at around 375 and 403 cm^{-1} corresponded to the in-plane E^1_{2g} and out-of-plane A_{1g} vibrational modes of the Mo−S bond in hexagonal MoS_2. In contrast with S220, the intensity of E^1_{2g} and A_{1g} peaks weakened, which was significantly correlated with a decreased crystal degree. In addition, a decreased crystal degree would shift and broaden E^1_{2g} and A_{1g} peaks. Beside E^1_{2g} and A_{1g} modes, generated peaks at about 284 and 334 cm^{-1} could be ascribed to the vibration modes of Mo−O bonds, demonstrating the oxygen doping with a decrease in synthesis temperature.[60] Peaks of the Mo−O bond in obtained samples were different from those in MoO_2 because of the different structures of the two kinds of materials. The peaks that appeared become more obvious with comparison of E^1_{2g} and A_{1g} modes as the synthesis temperature was decreased, suggesting an increase in oxygen dopant concentration. The related oxygen atomic concentration from EDS results and ratio of Mo−O bond from XPS results in Figure 1c verified that the doping oxygen content increased as the synthesis temperature dropped.

Atomic valence states and bonding configuration of obtained samples were determined by XPS. Characteristic peaks of Mo

https://doi.org/10.1021/acsnano.4c00691
ACS Nano 2024, 18, 7298−7310

Table 1. Kinetic Parameters for La(III) Recovery

	pseudo-first-order kinetic model			pseudo-second-order kinetic model		
	q_e (mg/(g·dm^2))	k_1 (min^{-1})	R^2	q_e (mg/(g·dm^2))	K_2 (min^{-1})	R^2
both	315.4409	0.0110	0.966	370.6622	0.00003382	0.989
cathode	79.8523	0.0186	0.926	90.2004	0.00002590	0.972
anode	50.7445	0.0190	0.934	57.0419	0.00004261	0.978

Table 2. Comparison of La(III) Recovery in the Work with Previous Literature

material	initial concentration (mg/L)	adsorption capacity (mg/g)	efficiency (mg/(g·min))	ref
Amberlite XAD-7 resin	200	7.342	0.041	68
Purolite S950	200	22.45	0.062	69
carbon nanotube	100	23.23	0.032	70
titanium oxide	100	12.31	0.035	71
activated carbon functionalized	50	10.14	0.051	72
$[Zn(bim)_2(bdc)]_n$ MOF	25	8.85	0.051	73
Ca−alginate Beads	25	6.373	0.004	74
GO composite	25	3.292	0.022	75
Fe_3O_4/GNPs	10	3.84	0.032	76
CEC with O-doped MoS_2	9.92	65.82	0.091	this work

3d, S 2p and O 1s appeared in the survey (Figure S2). The Mo 3d spectrum (Figure 1d) was fitted to the doublet peaks at ∼228.3 and 231.4 eV, corresponding to Mo^{4+} in Mo−S bonds, while the doublet peaks at ∼229.6 and 233.0 eV originated from the Mo^{6+} peaks for oxygen-doped $MoS_{2-x}O_x$.[61] Peaks affected by the generation of Mo−O bonds and decreased crystallinity shifted. The S 2p spectrum (Figure 1e) was divided into four sets of peaks, ∼162,5, 163.6, and 164.6 peaks, belonging to S $2p_{3/2}$, $2p_{1/2}$, and S_2^{2-}.[62] The formation of S_2^{2-} peaks could be attributed to the O doping of MoS_2.[63] In addition, the shift of peaks was due to varying crystallinity. In the O 1s spectrum (Figure 1f), the peak at ∼532.3 eV for S220 indicated adsorbed water.[64] With a decreasing synthesis temperature, the peak moved, and that situated at ∼530.2 eV was assigned to the Mo−O bond,[65] confirming that oxygen atoms were successfully incorporated into the structure of MoS_2.

With the aim of investigating the morphology of O-doped MoS_2, SEM-EDS (Figure S3) and TEM (Figure 1g) tests were carried out. All the samples possessed the nanoflower morphology with ultrathin nanosheets. Notably, the edges became obscurer as the synthesis temperature decreased, which suggested a lower crystallinity (in agreement with the results of XRD and Raman). Elemental Mo, S, and O were exhibited to be inert (Figure S3), indicating the existence of O atoms. SEM and the corresponding EDS diagram of O-doped MoS_2 (Figure S4), as well as the proportions of Mo, S, and O, showed the even distribution of all the elements and increased oxygen content as the synthesis temperature was decreased. Furthermore, structural characteristics of O-doped MoS_2 were researched according to HRTEM (Figure 1h). The distorted areas as marked in green circles demonstrated the generation of crystal defects, which would introduce the enhancement of conductivity.[66] A lattice fringe with a spacing of 0.625 nm belonged to the (002) plane of MoS_2. More crystal facets originating from MoS_2 were observed through a selected area electron diffraction (SAED) test (Figure 1i). Further, the TEM image and corresponding elemental mapping images (Figure 1j) of O-doped MoS_2 confirmed the presence of Mo, S, and O elements and the homogeneous distribution.

La(III) Recovery by CEC. The ability of an O-doped MoS_2 electrode through a CEC process to recover REEs was investigated. During the recovery process, O-doped MoS_2 was coated on a titanium plate as both the cathode and anode. As seen in the digital images (Figure S5), the electrode after recovery remained almost the same as that before use, revealing the stable coating of samples on a titanium plate. For comparison, the recovery abilities of electrodes with O-doped MoS_2 only as a cathode or anode or without O-doped MoS_2 electrodes were explored. The results displayed that O-doped MoS_2 as both cathode and anode performed the largest REE recovery, which reached an adsorption capacity (Figure 2a) of 365.71 mg/(g dm^2) and a corresponding recovery (Figure 2b) of 91.43%. Adsorption capacity (or recovery) using O-doped MoS_2 as both electrodes was more than 5- and 11-folds than that using O-doped MoS_2 as the cathode or anode, respectively, demonstrating that both electrodes being an O-doped MoS_2 electrode would enhance the transfer of ions in the solutions. The benefits of these dual-plate electrodes are rapid diffusion of targeted ions into the trench and improved specificity from two applied electrode potentials.[67] O-doped MoS_2 served as one electrode (cathode or anode) to study the recovery performance. Recovery by an O-doped MoS_2 cathode was higher than that of an O-doped MoS_2 anode, since the cathode was negatively charged, which benefited from the adsorption of positively charged La(III) through an electrostatic interaction. For a titanium plate without O-doped MoS_2, the adsorption capacity and recovery were almost zero, indicating that there was no interaction between targeted ions and the substrate. Besides, the pseudo-first-order model and the pseudo-second-order models were applied to study the adsorption process, and corresponding fitting data are exhibited in Table 1. The results showed that the adsorption process was well fitted by two models, including physical and chemical adsorption.

The La(III) recovery performance of at various initial concentrations was measured, in order to study the applicability (Figure 2c). As the increase initial concentration was increased, the adsorption increased and then reached a balance, while the recovery dropped with a concentration higher than 5 mg/L, demonstrating saturation of recovery sites.

https://doi.org/10.1021/acsnano.4c00691
ACS Nano 2024, 18, 7298−7310

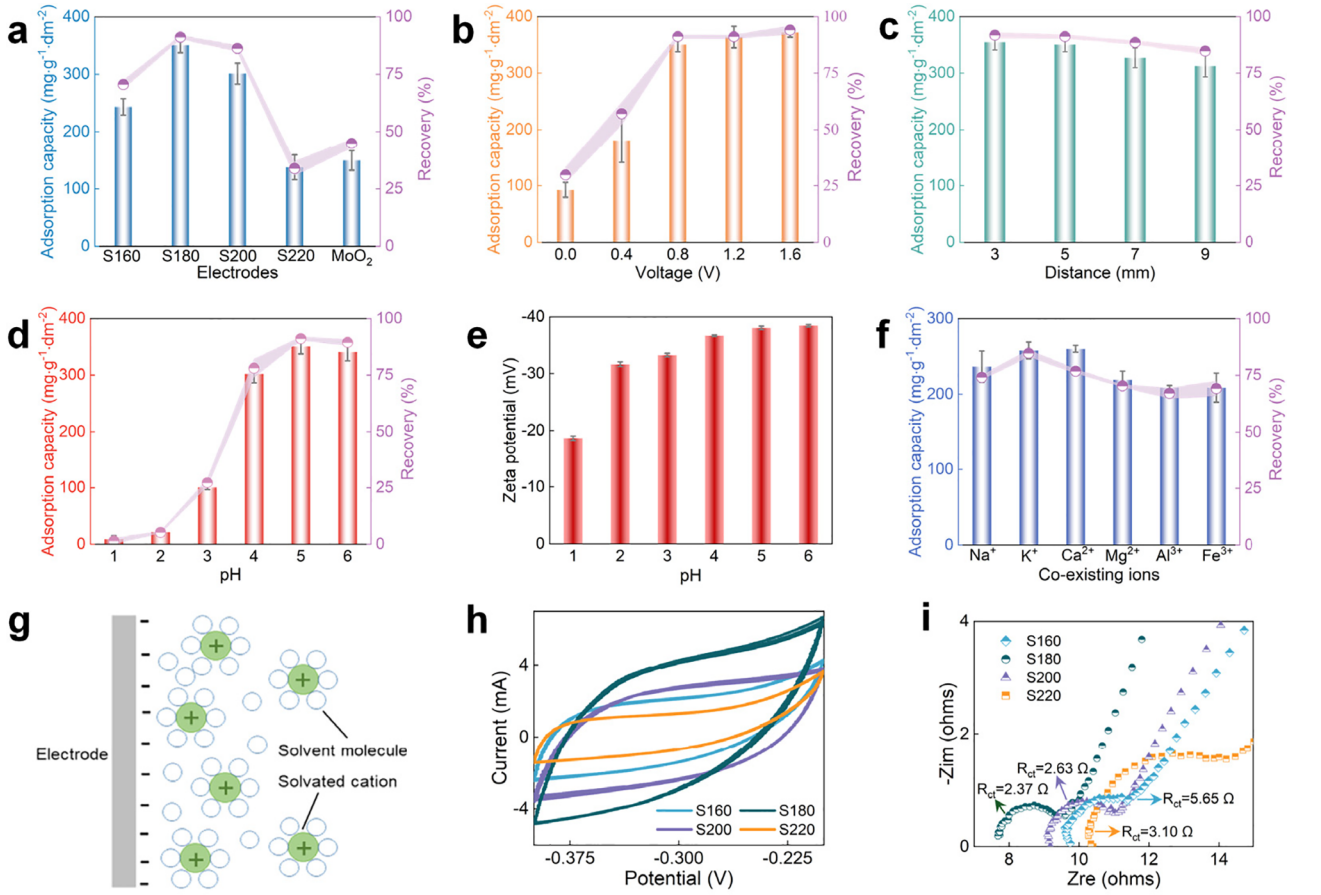

Figure 3. (a) Adsorption capacity and recovery of La(III) on MoS_2 and O-doped MoS_2 with different O doping concentrations. Effect of (b) charging voltage, (c) distance between two electrodes, and (d) pH on the CEC process of La(III) recovery. (e) Zeta potential of O-doped MoS_2 at various pHs. (f) Effect of the coexistence of ions on the recovery performance of La(III). (g) Schematic illustration of the electrical double layer for the storage of ions and the interaction between the electrode and ions. (h) CV curves of MoS_2 and O-doped MoS_2 in 1 M Na_2SO_4 solution. (i) EIS results of MoS_2 and O-doped MoS_2.

When the initial concentration was lower than 5 mg/L, an O-doped MoS_2 electrode could obtain a recovery of 100%. The recovery was higher than 90% within a low concentration range. In comparison with previous works, recovery efficiency based on adsorption capacity and recovery time was normalized, as displayed in Table 2, and this work exhibited superior recovery ability. The recovery mechanism of O-doped MoS_2 by CEC was studied by XPS. After recovery, the peaks for La(III) could be found in the survey spectrum (Figure S6). Species of O-doped MoS_2 existed in the electrode after La(III) recovery by the CEC process (Figure 2d–f). The slight shift of Mo 3d peaks for the anode might be attributed to oxidation (Figure 2d), while the changes appearing in S 2p (Figure 2e) and O 1s (Figure 2f) could be ascribed to the interaction between S and O atoms with La(III). Moreover, the peaks centered at ~832.92, ~851.8, and ~856.9 eV for La $3d_{5/2}$ and La $3d_{3/2}$ (Figure 2g) could be explained as the transfer of electrons from S or O atoms to La(III), thus forming an La–S or La–O coordination bond. All these results manifested that the O atoms and S atoms were the dominant sites for chemisorption of La(III). Apart from the above results about the adsorption of La(III), TEM and related elemental mapping of an O-doped MoS_2 sample after La(III) recovery confirmed the even distribution of Mo, S, O, and La (Figure 2h). According to the results of HRTEM (Figure S7), the structure of O-doped MoS_2 after recovery was almost identical to its prerecovery state. Therefore, La(III) could be successfully recovered by O-doped MoS_2 electrode through the CEC process.

Effects of Environmental Conditions and Ion Storage. MoS_2 and O-doped MoS_2 with various O doping concentrations as electrodes for La(III) recovery were investigated (Figure 3a). Note that incorporation of O atoms into MoS_2 strengthened the recovery of La(III), and the highest adsorption capacity and recovery were almost 1.45 and 2.25 times higher than that of MoS_2, respectively. The enhanced recovery might occur from improved affinity between the electrode with targeted ions and specific capacitance in the electrical double layer. Compared with the MoO_2 electrode, the adsorption capacity and recovery using the O-doped MoS_2 electrode were better. Because of the different crystal structures of MoS_2 and MoO_2, MoS_2 possessed better conductivity and surface area with sulfur atoms. REEs could be efficiently recovered through oxygen doping engineering on MoS_2 to improve electrochemical and chemical properties. La(III) recovery was reduced, since doping an excessive amount of oxygen atoms would weaken the specific capacitance for ion adsorption, as proved in previous work.[77] After that, the charging voltage on the CEC process of recovery was researched. Figure 3b presents the adsorption capacity and recovery of La(III) at various applied voltages. Here, it could be seen that La(III) recovery was enhanced quickly upon

https://doi.org/10.1021/acsnano.4c00691
ACS Nano 2024, 18, 7298–7310

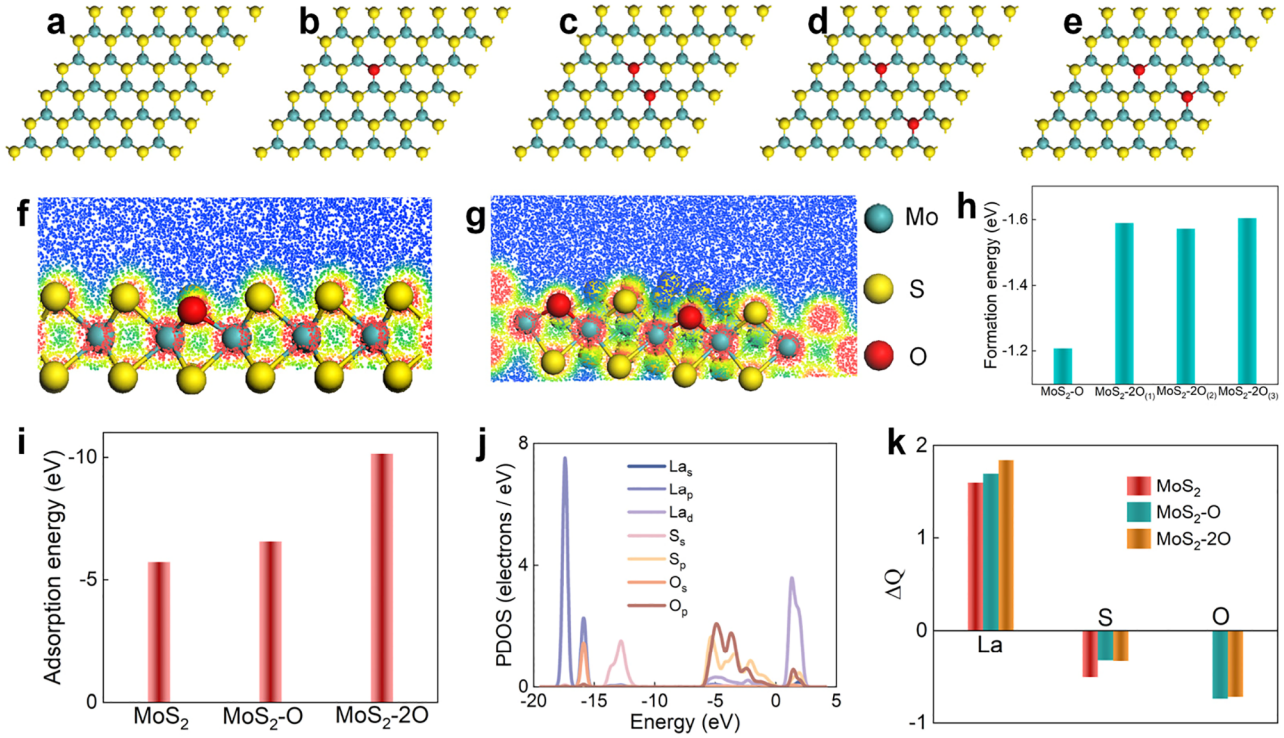

Figure 4. Top views of the supercell models of (a) MoS_2, (b) MoS_2-O, (c) MoS_2-$2O_{(1)}$, (d) MoS_2-$2O_{(2)}$, and (e) MoS_2-$2O_{(3)}$. Electron density maps of (f) MoS_2−O and (g) MoS_2-2O. (h) Formation energy of MoS_2 and O-doped MoS_2. (i) Adsorption energy between La(III) and MoS_2 (or O-doped MoS_2). (j) PDOS of La(III), S, and O in the system of La(III) adsorption on O-doped MoS_2. (k) Mulliken atomic charge changes of La(III), S, and O in the system of La(III) adsorption on O-doped MoS_2.

applying the charging voltage and then tended to a stable stage, indicating the occurrence of a strong electrostatic interaction at the beginning and then reached saturation of adsorption sites on the O-doped MoS_2 electrode. The effect of distance between two electrodes on La(III) recovery was employed (Figure 3c). Adsorption capacity and recovery declined with the increase of distance. At a greater distance, the resistance between two electrodes was enhanced, and an electrical double layer was induced. As a result, the adsorption capacity and recovery ability were reduced. The influence of pH on La(III) recovery was studied (Figure 3d). At a higher pH, a higher La(III) recovery by the CEC process was achieved, which was due to the less active sites occupied by H^+. Apart from the above variants, with an increase of pH, O-doped MoS_2 possessed more negative charges, favoring the adsorption of La(III) according to an electrostatic interaction (Figure 3e). The balance of recovery was due to the saturation of active sites. To evaluate the application of the CEC method with an actual O-doped MoS_2 electrode, recovery of La(III) was tested in a binary mixed solution (Figure 3f). As could be found, the adsorption capacity and recovery were minimally affected, and ions with higher valence exhibited stronger competition with La(III). In any event, the adsorption capacity and recovery remained at a high level.

The CEC process for ion recovery (Figure 3g) is related to the electrical double layer for storage of ions and interaction between electrode and ions. Here, the electrochemical performances of MoO_2, MoS_2, and O-doped MoS_2 electrodes were tested by CV in a 1 M Na_2SO_4 solution (Figure S8 and Figure 3h). The results showed that MoS_2 and O-doped MoS_2 obtained a good capacitance property, and the capacitance first increased and then decreased with the enhanced O doping concentration. Among these materials, S180 exhibited the best adsorption capacity. Better ion storage ability appeared on the O-doped MoS_2 electrode than that on the MoO_2 electrode. Further, the resistance of ion transfer was examined through an EIS test (Figure 3i and Figure S9). The calculated charge-transfer resistances (R_{ct}) based on the circuit were 5.65, 3.10, 2.37, and 2.63 Ω for S160, S180, S200, and S220, respectively. Compared with R_{ct} of MoO_2 at 76.56 Ω (Figure S9), all the MoS_2 and O-doped MoS_2 electrodes had a lower ion transfer ability. Moreover, it was revealed that the incorporation of O atoms would reduce the ion transfer resistance, where S180 had the smallest charge transfer resistance among MoS_2 and O-doped MoS_2 electrodes due to its good electric conductivity. The improved contact resistance was attributed to formation of an Mo−O bond with a lower Schottky barrier compared with an Mo−S bond.[78] After oxygen doping, the disordered structure generated more active unsaturated sulfur atoms, thus tuning the electronic structure.[79] A decline of R_{ct} from S160 to S180 originated from the decreased disorder degree. The above results demonstrated that O-doped MoS_2 had a better electrical double layer for ions storag and lower resistance for an ion transfer.

Interaction in CEC Process. To account for the interaction performance between La(III) and O-doped MoS_2, DFT was adopted to consider adsorption of La(III) on different O doping concentrations of MoS_2. First, MoS_2 and the possible structure of O-doped MoS_2 were optimized (Figure 4a−e). According to the related electron density maps of O-doped MoS_2 (Figure 4f,g) with different doping concentrations, it was demonstrated that O atoms could strongly bind with Mo atoms. The shift of doped atoms was related to the atomic volume, and O shifted inward because of

https://doi.org/10.1021/acsnano.4c00691
ACS Nano 2024, 18, 7298−7310

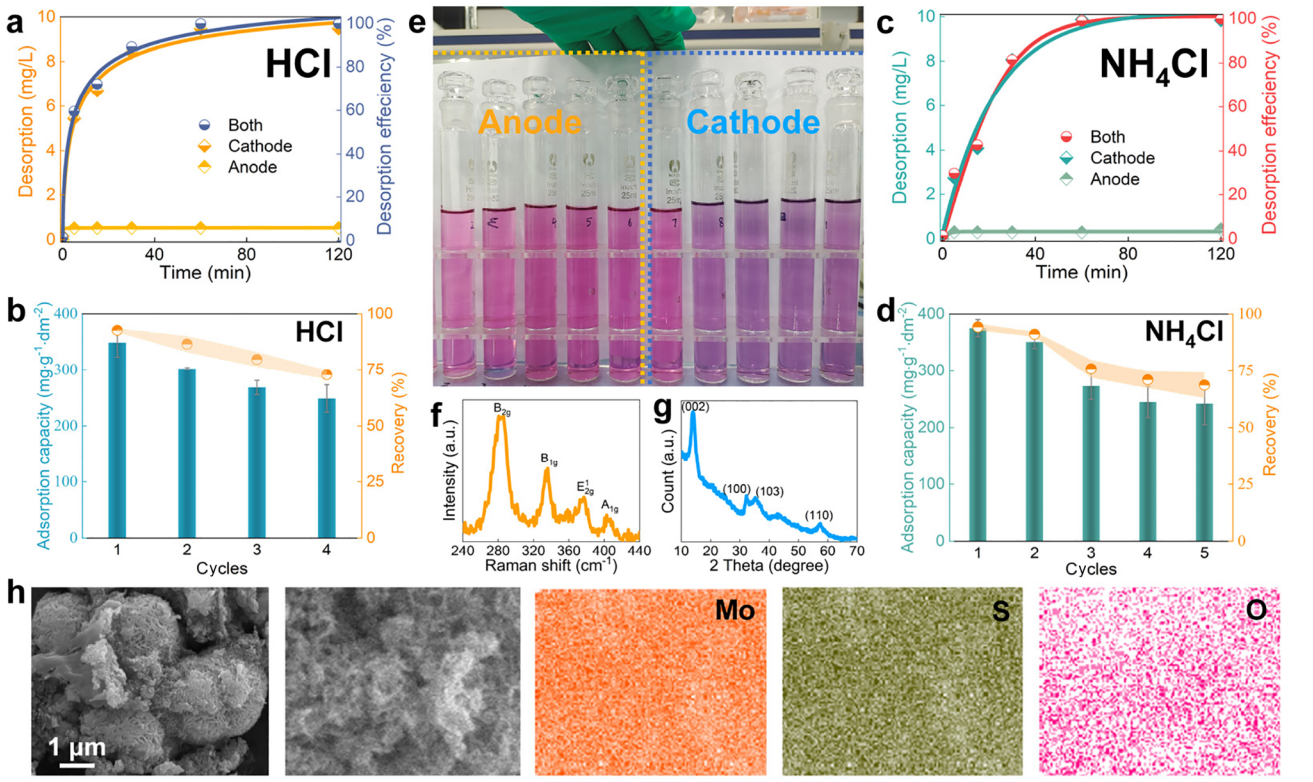

Figure 5. (a) Desorption of La(III) from an O-doped MoS_2 electrode by HCl and (b) related recovery cycles. (c) Desorption of La(III) from O-doped MoS_2 electrode by NH_4Cl and (d) related recovery cycles. (e) Color comparison of anode and cathode after desorption. (f) XRD pattern and (g) Raman spectrum of O-doped MoS_2 after desorption. (h) SEM images and corresponding elemental mapping: Mo, S, and O of O-doped MoS_2 after the desorption of La(III).

the smaller volume compared with that of S.[80] Besides, the Mo−O bond length was shorter than that of Mo−S, which was ascribed to the stronger electronegativity of O atoms. With more O atom doping, the structure of O-doped MoS_2 became more distorted, consistent with the experimental results. The formation energy was calculated to further investigate the stability of O-doped MoS_2 (Figure 4h). Negative formation energy exhibited the possibility of a spontaneous reaction for O doping. The highest absolute value of formation energy was MoS_2-$2O_{(3)}$ in MoS_2 with two substituted S atoms by O atoms, indicating its status as the most stable structure at this doping concentration. In a subsequent adsorption study, MoS_2-$2O_{(3)}$ was utilized as the model for the incorporation of the doping of two O atoms.

The calculated interaction energies of La(III) and MoS_2 with and without O incorporation are displayed in Figure 4i. The adsorption energy between La(III) and O-doped MoS_2 was superior to that of MoS_2. The adsorption energy was enhanced with doping of more oxygen atoms, showing that the incorporated O atoms had a strong interaction ability with La(III). To figure out the reason for the decreased recovery at high concentration, the adsorption energies between various concentrations of La(III) and O-doped MoS_2 were calculated (Figure S10). The interaction between La(III) and O-doped MoS_2 was strengthened at first and then plateaued. As a consequence, in a high-concentration situation, La(III) recovery will decrease, but adsorption capacity was apt to balance. In addition to this, there was repulsion among La(III) because of electrostatic forces with the same positive charges. With adsorption of more La(III), a stronger interaction between targeted ions and electrodes should be considered. Moreover, interacting orbitals of La(III) and S (or O atoms) were used to further clarify the adsorption process (Figure 4j). s, p, and d orbitals in La(III) bound strongly with S p and O s and p orbitals, demonstrating the interaction between La and S, O atoms. Compared with the results in MoS_2 without (Figure S11) and with a greater O doping concentration (Figure S12) system, interaction between MoS_2 and La(III) was enhanced as more O atoms were introduced. Based on Mulliken atomic charge changes (ΔQ) (Figure 4k), the charge changes between La(III) and MoS_2 (or O-doped MoS_2) before and after adsorption were calculated. Lost charges of La(III) transferred to nearby S or O atoms, exhibiting the tough interaction between La(III) and S or O atoms. To obtain an insight into the adsorption sites of O and S atoms, the view after adsorption is provided in Figure S13. The distance between La(III) and O atoms was closer than that with an S atom, illustrating a stronger interaction of La(III) and O atoms, owing to greater electronegativity.[81,82] The phenomenon was also demonstrated by the higher atomic charge transfer of an O atom. Compared with the MoS_2 system, the higher positive charge of La(III) originated from the stronger interaction than that in the O-doped MoS_2 system. And the promoted interaction in O-doped MoS_2 was due to the interaction between La(III) and O atoms. The above results proved that the incorporation of oxygen atoms would strengthen the chemical interaction of La(III) and MoS_2.

Adsorption and Desorption Cycles. The reusability of materials is crucial to the application of the CEC process. Here, desorption of La(III) from O-doped MoS_2 was investigated using HCl and NH_4Cl. It turned out that HCl (Figure 5a) and NH_4Cl (Figure 5c) could efficiently desorb

https://doi.org/10.1021/acsnano.4c00691
ACS Nano 2024, 18, 7298−7310

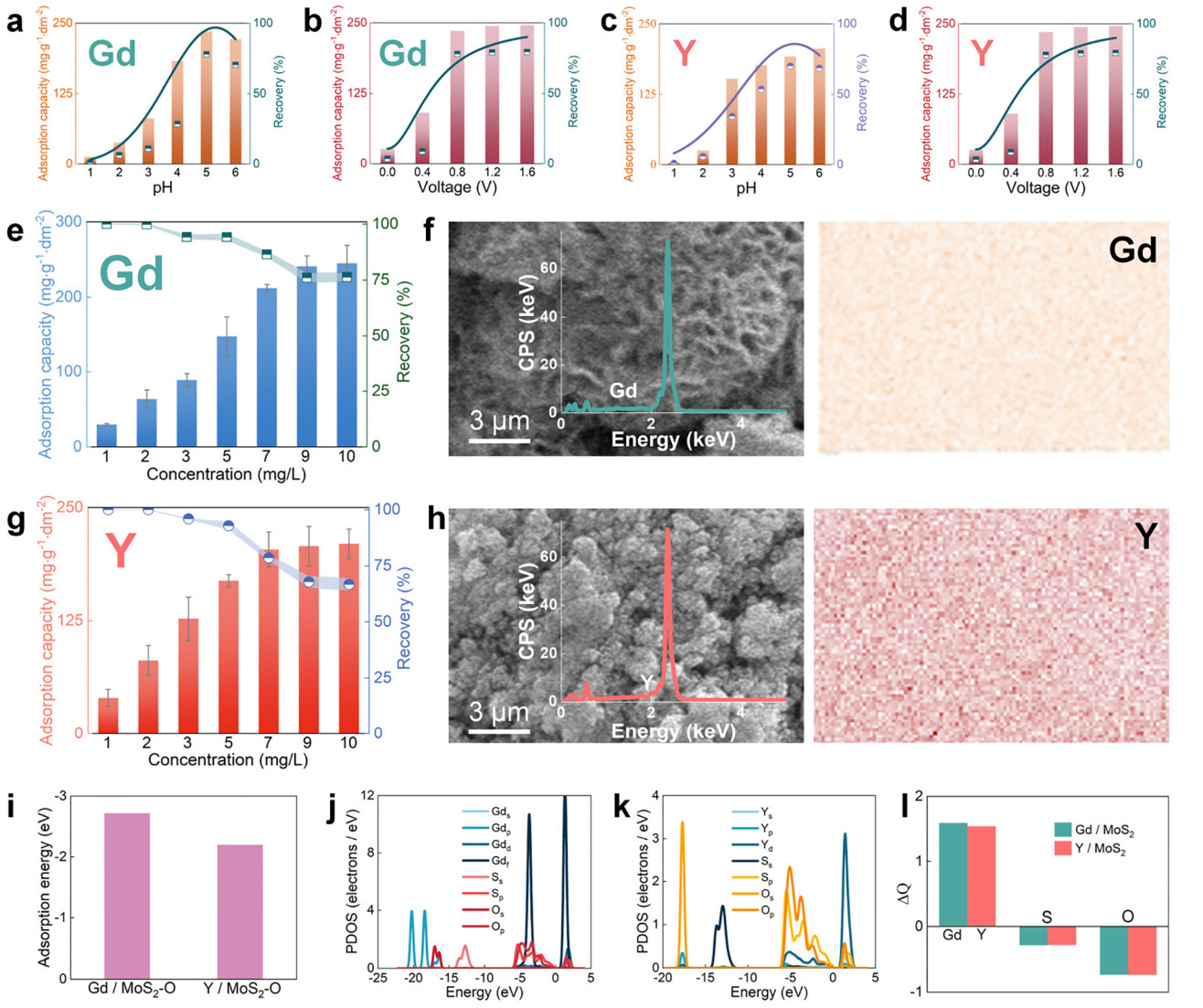

Figure 6. Effect of pH, and voltage on (a, b) Gd(III) and (c, d) Y(III) recovery by an O-doped MoS_2 electrode. Adsorption capacity and recovery of (e) Gd(III) and (g) Y(III) at various initial concentrations. SEM and related elemental mapping of O-doped MoS_2 electrode after (f) Gd(III) and (h) Y(III) recovery. (i) Adsorption energy between Gd(III) (or Y(III)) and O-doped MoS_2. (j) PDOS of Gd(III), S, and O in the system of Gd(III) adsorption on O-doped MoS_2. (k) PDOS of Y(III), S and O in the system of Y(III) adsorption on O-doped MoS_2. (l) Mulliken atomic charge changes of Gd(III) (or Y(III)), S and O in the system of Gd(III) (or Y(III)) adsorption on O-doped MoS_2.

La(III) from the O-doped MoS_2 electrode. At approximately 60 min, the total desorption efficiency exceeded 90%. The total desorption and corresponding desorption efficiency reached almost 10 mg/L and 100% within 120 min, respectively. Judging from the color of the desorption solutions (Figure 5e), it changed from dark to light color for the desorption of the cathode, which meant that the adsorption of La(III) was mainly completed on the cathode, and the results were also confirmed by the desorption efficiency. Subsequently, the consecutive cycles of the O-doped MoS_2 electrode using HCl (Figure 5b) and NH_4Cl (Figure 5d) for desorption were studied. During the repeated experiment, small amounts of the samples were dropped in all solutions, resulting in a decreased recovery performance. With an increase in the adsorption and desorption cycles, the adsorption capacity and recovery dropped, demonstrating that the desorption would destroy the active sites of O-doped MoS_2. Besides, the results proved that the interaction between La(III) and O-doped MoS_2 could be attributed to physical and chemical sorption. However, the adsorption and desorption cycle performance using NH_4Cl was better than that by HCl, originating from the instability of MoS_2 in acid solution. After adsorption and desorption cycles, the crystal structure (Figure 5f) and bonding component (Figure 5g) of O-doped MoS_2 were still consistent with those before, indicating that the method to desorb La(III) from O-doped MoS_2 did not damage the whole structure. Moreover, morphology and elemental distribution (Figure 5h) of O-doped MoS_2 were not destroyed, which exhibited the good recyclability of the O-doped MoS_2 electrode. The method favorably contributed to a better understanding of the desorption process and provided valuable guidance to the recovery of REEs and reusability to achieve the actual application.

Recovery of Other REEs. Furthermore, the performances by O-doped MoS_2 electrode in the CEC process for recovery of other REEs were explored (Figure S14). It revealed that all REEs could be recovered through an O-doped MoS_2 electrode in the CEC process, with good recovery. Different REE

https://doi.org/10.1021/acsnano.4c00691
ACS Nano 2024, 18, 7298−7310

recovery behaviors were related with their outer nuclear electron shell and formation of ions in aqueous solutions. Here, Gd(III) and Y(III) were chosen as medium and heavy REEs to study more recovery behaviors using an O-doped MoS_2 electrode. The adsorption capacity of Gd(III) and Y(III) in Figures S15 and S16 showed a similar increasing trend with time compared with that of La(III). The pseudo-first-order model and the pseudo-second-order models for fitting by O-doped MoS_2 and MoO_2 electrodes are exhibited in Tables S1 and S2, respectively. This revealed that the adsorption processes for Gd(III) and Y(III) were physical and chemical adsorption. As well, adsorption capacity and recovery using O-doped MoS_2 were better than that by MoO_2. Factors affecting Gd(III) and Y(III) recovery including pH and voltage were studied. As displayed in Figure 6a,c, the similar tendency of recovery resulted from an enhanced electrostatic interaction of La(III) and O-doped MoS_2. For recovery under various voltage values (Figure 6b,d), a higher electrostatic interaction would be strengthened between electrode and REEs.

In Figure 6e,g, the results showed that adsorption capacities of Gd(III) and Y(III) were 176 and 170 mg/(g dm^2) at an initial concentration of 5 mg/L, and related recoveries were 95.6% and 93.1%, respectively. With an increase in the initial concentration, the adsorption capacity and recovery decreased, resulting from the limited ion storage in the electrical double layer. When the initial concentration was lower than 5 mg/L, the recovery achieved 100%, which exhibited excellent recovery of rare earth elements in the low concentration range. According to the results of SEM and related elemental mapping (Figure 6f,h), Gd(III) and Y(III) recoveries on the surface of O-doped MoS_2 electrode were demonstrated. In comparison with previous works, as shown in Tables S3 and S4, the Gd(III) and Y(III) recovery ability using the O-doped MoS_2 electrode was better.

To further verify the interaction between Gd(III), Y(III), and doped MoS_2, DFT was applied. The adsorption energy of Y(III) and O-doped MoS_2 was lower than that of Y(III) of O-doped MoS_2 (Figure 6i), and the binding energy with La(III) (Figure 4i) was the lowest. The higher interaction strengthened the recovery of REEs by the CEC process. Besides, interaction of Gd(III) and Y(III) in high concentration with O-doped MoS_2 is given in Figures S17 and S18, respectively. A similar phenomenon with enhancing and balancing interaction was observed, originating from limited adsorption sites. With the purpose of investigating the binding orbitals between Gd(III) or Y(III) and O-doped MoS_2, the PDOS of Gd(III), Y(III), and nearby S and O atoms are exhibited in Figure 6j,k. Whether it was La(III), Gd(III), or Y(III), REEs could bind tightly with S and O atoms on the surface of O-doped MoS_2. Compared with Y(III) and La(III) (Figure 4j), f orbitals in Gd(III) participated in the interaction with S and O atoms, which enhanced the chemisorption of Gd(III) to some extent. The more negatively charged O atom in comparison to the S atom demonstrated that interactions between Y(III) or Gd(III) with O atoms were stronger than those with S atoms, which could be seen in the closer distance of REEs and the O atom in Figure S13 as well. Moreover, Mulliken atomic charge changes showed that REEs connect with S and O atoms (Figure 6l), and Gd(III) bound to O-doped MoS_2 more strongly than Y(III). The greater force between the S atoms may be attributed to the higher atomic charge changes in Gd(III).

CONCLUSION

The recovery of REEs from aqueous solutions in low concentrations based on the design of an O-doped MoS_2 electrode was proposed. The CEC process with an O-doped MoS_2 electrode reached an REE recovery of ~100% when the initial concentration was at a certain value. A maximum adsorption capacity of REEs of 365.71 mg/(g dm^2) was obtained. In a multicomponent solution, the adsorption capacity and recovery were slightly affected. The parameters of the CEC process, including pH, applied voltage, distance between electrodes, and initial concentrations, were investigated in detail. The efficient recovery of REEs could be attributed to the enhanced transfer rate and electrical double layer thinness for REE storage. Further, the strong interaction between doped O atoms and REEs helped strengthen the chemical interaction. The REE recovery was impacted by different binding forces between REEs and O-doped MoS_2. Apart from the above results, the desorption efficiency from the O-doped MoS_2 electrode reached ~100% within 120 min, and the electrode exhibited good stability. Therefore, this study proposed a process to recover REEs from aqueous solutions and could be used to shed some light on resource recycling and environmental applications.

METHODS

Samples and Electrode Preparation. A hydrothermal treatment was carried out using a 100 mL Teflon-lined stainless-steel autoclave to synthesize MoS_2 at 220 °C. Different O doping concentrations were controlled by adjusting the synthesis temperature (200, 180, and 160 °C). 2 mmol of $(NH_4)_6Mo_7O_{24}{\cdot}4H_2O$ and 60 mmol of CN_2H_4S were dissolved in 72 mL of distilled water with stirring. After this, the solution was transferred a 100 mL Teflon-lined stainless-steel autoclave at various temperatures for 24 h. Afterward, after cooling to normal temperature, the products were collected by filtration and washed using water and ethanol. Finally, they were dried by freeze-drying at −60 °C in vacuum. The incorporation of O atoms into the structure of MoS_2 could be easily achieved by adjusting the temperature (200, 180, and 160 °C) during the hydrothermal process. The prepared samples were denoted as S220, S200, S180, and S160 according to the variable temperature. Electrodes were prepared through coating samples on the surface of titanium plates (more details are provided in the Supporting Information).

Experimental Design. REE recovery experiments were performed in a self-made cell with an external power supply, and a 200 mL solution with a certain REE concentration and pH was pumped at a rate of 45 rpm through a peristaltic pump (YZ1515x, China). There was no adjustment of the solution pH during the whole operation. REE concentrations were measured using an Origin Aquamate 8000 UV−vis spectrophotometer (Lambda 750S). The test solution was collected at predetermined time intervals from the cell, and the corresponding recovery performances were evaluated via adsorption capacity (Q) and recovery (R) as

$$Q = \frac{C_0V_0 - C_tV_t}{Am} \tag{1}$$

$$R = \frac{C_0 - C_t}{C_0} \times 100\% \tag{2}$$

where C_0 and C_t represent the REE concentrations at the initial and t moments during the recovery operations, respectively (in mg/L), V_0 and V_t are the volumes of REE solution at the initial and t moments respectively (in L), A exhibited the effective surface area with samples on the surface of the electrode (in dm^2), and m is the mass of samples used in the mixture of electrodes (in mg).

Simulations. Interaction between REEs and oxygen-doped MoS_2 was calculated based on density functional theory calculations

https://doi.org/10.1021/acsnano.4c00691
ACS Nano 2024, 18, 7298−7310

(DMol3 program). The exchange and correlation between electrons were described by the Generalized Gradient Approximation (GGA) formulated by Perdew–Burke–Ernzerhof (PBE). The cutoff energy for auxiliary plane waves was set to 340 eV.The Brillouin zone was sampled by 5 × 5 × 1 *k*-points for the optimization of the model. A vacuum length of 20 Å was used to avoid the interaction between the neighboring images. With the aim of investigating REE recovery performance on O-doped MoS_2 in high concentration, various numbers of REEs (1, 2, 3, 4) werewas applied. The tability of O-doped MoS_2 was characterized according to the formation energies as

$$E_{form} = E_{doped} - E_{pure} + \mu_S - \mu_O \quad (3)$$

where E_{form} is the formation energy, E_{doped} and E_{pure} represent the total energy of O-doped MoS_2 and MoS_2, respectively, and μ_S and μ_O are the chemical potentials of S and O atoms, respectively.

The adsorption energy of La(III) on MoS_2 (or O-doped MoS_2) was calculated as

$$E_{ads} = E_{adsorbent+La(III)} - E_{adsorbent} - E_{La(III)} \quad (4)$$

in which E_{ads} is the adsorption energy between La(III) and MoS_2 (or O-doped MoS_2), $E_{adsorbent+La(III)}$ is the total energy after adsorption of La(III) on MoS_2 (or O-doped MoS_2), $E_{adsorbent}$ is the energy of MoS_2 (or O-doped MoS_2), and $E_{La(III)}$ is the energy of La(III).

Reusability. Desorption of La(III) from an O-doped MoS_2 electrode was performed in 1 M HCl (or 1 M NH_4Cl). The desorption efficiency was calculated as

$$D = \frac{C_d}{C_0} \times 100\% \quad (5)$$

In which C_d is the concentration of La(III) in HCl (or NH_4Cl) solution during the desorption process (in mg/L).

ASSOCIATED CONTENT

Supporting Information

The Supporting Information is available free of charge at https://pubs.acs.org/doi/10.1021/acsnano.4c00691.

Experimental methods (which contains details of materials used in this work, more details regarding electrode preparation, and materials characterizations), XRD spectrum, CV scan, and EIS of MoO_2, XPS survey, SEM, and corresponding EDS diagrams of prepared samples, digital images of electrodes before and after use, survey spectrum and TEM images of electrode after REE recovery, adsorption energy between various concentrations of REEs on O-doped MoS_2, PDOS of REE adsorption on MoS_2 and MoS_2-2O, view of REE adsorption on O-doped MoS_2, recovery of more REEs by O-doped MoS_2 electrode, adsorption capacity and corresponding kinetic parameters of Gd(III) and Y(III) on O-doped MoS_2 and MoO_2 electrode, and comparison of Gd(III) and Y(III) recovery in this work with previous literatures (PDF)

AUTHOR INFORMATION

Corresponding Authors

Shaoxian Song − *Key Laboratory of Green Utilization of Critical Non-metallic Mineral Resources of Ministry of Education, Wuhan, Hubei 430070, People's Republic of China; Hubei Key Laboratory of Mineral Resources Processing and Environment, Wuhan University of Technology, Wuhan, Hubei 430070, People's Republic of China;* orcid.org/0000-0001-7278-7875; Email: ssx851215@whut.edu.cn

Feifei Jia − *Key Laboratory of Green Utilization of Critical Non-metallic Mineral Resources of Ministry of Education, Wuhan, Hubei 430070, People's Republic of China; Hubei Key Laboratory of Mineral Resources Processing and Environment, Wuhan University of Technology, Wuhan, Hubei 430070, People's Republic of China;* orcid.org/0000-0003-0427-8117; Email: feifeijia@whut.edu.cn

Authors

Weiquan Zhan − *Key Laboratory of Green Utilization of Critical Non-metallic Mineral Resources of Ministry of Education, Wuhan, Hubei 430070, People's Republic of China; Hubei Key Laboratory of Mineral Resources Processing and Environment, Wuhan University of Technology, Wuhan, Hubei 430070, People's Republic of China; Instituto de Fisica, Universidad Autonoma de San Luis Potosi, C.P. 78290 San Luis Potosi, S.L.P., Mexico;* orcid.org/0000-0002-3116-2737

Xuan Zhang − *Key Laboratory of Green Utilization of Critical Non-metallic Mineral Resources of Ministry of Education, Wuhan, Hubei 430070, People's Republic of China; Hubei Key Laboratory of Mineral Resources Processing and Environment, Wuhan University of Technology, Wuhan, Hubei 430070, People's Republic of China*

Yuan Yuan − *Key Laboratory of Green Utilization of Critical Non-metallic Mineral Resources of Ministry of Education, Wuhan, Hubei 430070, People's Republic of China; Hubei Key Laboratory of Mineral Resources Processing and Environment, Wuhan University of Technology, Wuhan, Hubei 430070, People's Republic of China; Doctorado Institucional de Ingeniería y Ciencia de Materiales, Universidad Autonoma de San Luis Potosi, San Luis Potosi 78210, Mexico*

Qizheng Weng − *Key Laboratory of Green Utilization of Critical Non-metallic Mineral Resources of Ministry of Education, Wuhan, Hubei 430070, People's Republic of China; Hubei Key Laboratory of Mineral Resources Processing and Environment, Wuhan University of Technology, Wuhan, Hubei 430070, People's Republic of China*

María de Jesús Martínez-López − *Universidad de la Costa, Carretera al Libramiento Paraje de Las Pulgas, C.P. 71600 Santiago Pinotepa Nacional, Mexico*

José Luis Arauz-Lara − *Instituto de Fisica, Universidad Autonoma de San Luis Potosi, C.P. 78290 San Luis Potosi, S.L.P., Mexico*

Complete contact information is available at: https://pubs.acs.org/10.1021/acsnano.4c00691

Author Contributions

W.Z. designed and performed the experiments, and the theoretical calculations, analyzed data, and wrote the original draft. X.Z., Y.Y., and Q.W. aided in experiments. M.d.J.M.-L. and J.L.A.-L. aided in data analysis. S.S. and F.J. helped in data analysis and edited the manuscript.

Notes

The authors declare no competing financial interest.

ACKNOWLEDGMENTS

The work was financially supported by the National Key Research and Development Program of China (2021YFC2900900) and the Natural Science Foundation of

Hubei Province (ZRJQ2022000195). W.Z. gratefully acknowledges the Consejo Nacional de Humanidades Ciencias y Tecnologías (CONAHCYT) of Mexico for offering him a scholarship under grant No. 813934 during his Ph.D. study.

REFERENCES

(1) Ji, H.; Wu, J.; Cai, Z.; Liu, J.; Kwon, D. H.; Kim, H.; Urban, A.; Papp, J. K.; Foley, E.; Tian, Y.; Balasubramanian, M.; Kim, H.; Clément, R. J.; McCloskey, B. D.; Yang, W.; Ceder, G. Ultrahigh Power and Energy Density in Partially Ordered Lithium-Ion Cathode Materials. *Nature Energy* **2020**, *5* (3), 213−221.

(2) Bombelli, P.; Savanth, A.; Scarampi, A.; Rowden, S. J. L.; Green, D. H.; Erbe, A.; Årstøl, E.; Jevremovic, I.; Hohmann-Marriott, M. F.; Trasatti, S. P.; Ozer, E.; Howe, C. J. Powering a Microprocessor by Photosynthesis. *Energy Environ. Sci.* **2022**, *15* (6), 2529−2536.

(3) Zeng, Z.; Xu, Y.; Zhang, Z.; Gao, Z.; Luo, M.; Yin, Z.; Zhang, C.; Xu, J.; Huang, B.; Luo, F.; Du, Y.; Yan, C. Rare-Earth-Containing Perovskite Nanomaterials: Design, Synthesis, Properties and Applications. *Chem. Soc. Rev.* **2020**, *49* (4), 1109−1143.

(4) Kostelnik, T. I.; Orvig, C. Radioactive Main Group and Rare Earth Metals for Imaging and Therapy. *Chem. Rev.* **2019**, *119* (2), 902−956.

(5) Waldherr, G.; Wang, Y.; Zaiser, S.; Jamali, M.; Schulte-Herbrüggen, T.; Abe, H.; Ohshima, T.; Isoya, J.; Du, J. F.; Neumann, P.; Wrachtrup, J. Quantum Error Correction in a Solid-State Hybrid Spin Register. *Nature* **2014**, *506* (7487), 204−207.

(6) Förster, S. C.; Heinze, K.; Pandey, R. K.; Ng, D. K. P.; Torres, T.; Dumoulin, F.; Fö, C. Photophysics and Photochemistry with Earth-Abundant Metals − Fundamentals and Concepts. *Chem. Soc. Rev.* **2020**, *49* (4), 1057−1070.

(7) Borst, A. M.; Smith, M. P.; Finch, A. A.; Estrade, G.; Villanova-de-Benavent, C.; Nason, P.; Marquis, E.; Horsburgh, N. J.; Goodenough, K. M.; Xu, C.; Kynický, J.; Geraki, K. Adsorption of Rare Earth Elements in Regolith-Hosted Clay Deposits. *Nat. Commun.* **2020**, *11* (1), 1−15.

(8) Alonso, E.; Sherman, A. M.; Wallington, T. J.; Everson, M. P.; Field, F. R.; Roth, R.; Kirchain, R. E. Evaluating Rare Earth Element Availability: A Case with Revolutionary Demand from Clean Technologies. *Environ. Sci. Technol.* **2012**, *46* (6), 3406−3414.

(9) Fan, M. C.; Wozny, J.; Gong, J.; Kang, Y. Q.; Wang, X. S.; Zhang, Z. X.; Zhou, G. M.; Zhao, Y.; Li, B. H.; Kang, F. Y. Lithium Metal Recycling from Spent Lithium-Ion Batteries by Cathode Overcharging Process. *Rare Metals* **2022**, *41* (6), 1843−1850.

(10) Zheng, B.; Fan, J.; Chen, B.; Qin, X.; Wang, J.; Wang, F.; Deng, R.; Liu, X. Rare-Earth Doping in Nanostructured Inorganic Materials. *Chem. Rev.* **2022**, *122* (6), 5519−5603.

(11) Bian, Y. Y.; Guo, S. Q.; Xu, Y. L.; Tang, K.; Lu, X. G.; Ding, W. Z. Recovery of Rare Earth Elements from Permanent Magnet Scraps by Pyrometallurgical Process. *Rare Metals* **2022**, *41* (5), 1697−1702.

(12) Kegl, T.; Košak, A.; Lobnik, A.; Novak, Z.; Kralj, A. K.; Ban, I. Adsorption of Rare Earth Metals from Wastewater by Nanomaterials: A Review. *J. Hazard Mater.* **2020**, *386*, No. 121632.

(13) Naidu, G.; Ryu, S.; Thiruvenkatachari, R.; Choi, Y.; Jeong, S.; Vigneswaran, S. A Critical Review on Remediation, Reuse, and Resource Recovery from Acid Mine Drainage. *Environ. Pollut.* **2019**, *247*, 1110−1124.

(14) Zou, D.; Li, H.; Deng, Y.; Chen, J.; Bai, Y. Recovery of Lanthanum and Cerium from Rare Earth Polishing Powder Wastes Utilizing Acid Baking-Water Leaching-Precipitation Process. *Sep Purif Technol.* **2021**, *261*, No. 118244.

(15) Binnemans, K.; Jones, P. T.; Blanpain, B.; Van Gerven, T.; Yang, Y.; Walton, A.; Buchert, M. Recycling of Rare Earths: A Critical Review. *J. Clean Prod* **2013**, *51*, 1−22.

(16) Wang, K.; Adidharma, H.; Radosz, M.; Wan, P.; Xu, X.; Russell, C. K.; Tian, H.; Fan, M.; Yu, J. Recovery of Rare Earth Elements with Ionic Liquids. *Green Chem.* **2017**, *19* (19), 4469−4493.

(17) Hermassi, M.; Granados, M.; Valderrama, C.; Ayora, C.; Cortina, J. L. Recovery of Rare Earth Elements from Acidic Mine Waters: An Unknown Secondary Resource. *Science of The Total Environment* **2022**, *810*, No. 152258.

(18) Li, Z.; Li, X.; Raiguel, S.; Binnemans, K. Separation of Transition Metals from Rare Earths by Non-Aqueous Solvent Extraction from Ethylene Glycol Solutions Using Aliquat 336. *Sep Purif Technol.* **2018**, *201*, 318−326.

(19) Ramasamy, D. L.; Porada, S.; Sillanpää, M. Marine Algae: A Promising Resource for the Selective Recovery of Scandium and Rare Earth Elements from Aqueous Systems. *Chemical Engineering Journal* **2019**, *371*, 759−768.

(20) Omodara, L.; Pitkäaho, S.; Turpeinen, E. M.; Saavalainen, P.; Oravisjärvi, K.; Keiski, R. L. Recycling and Substitution of Light Rare Earth Elements, Cerium, Lanthanum, Neodymium, and Praseodymium from End-of-Life Applications - A Review. *J. Clean Prod* **2019**, *236*, No. 117573.

(21) Bao, X.-j.; Zhang, Z.-j.; Luo, T.-z.; Wu, X.-t.; Xie, Z.-s.; Lan, S.-k.; Xie, S.-z.; Zhou, D.-b. Conversion of Cerium and Lanthanum from Rare Earth Polishing Powder Wastes to CeO_2 and $La_{0.6}Ca_{0.4}CoO_3$. *Hydrometallurgy* **2020**, *193*, No. 105317.

(22) Yu, B. S.; Jiang, J. L.; Yang, C. C. Conversion of Lanthanum and Cerium Recovered from Hazardous Waste Polishing Powders to Hazardous Ammonia Decomposition Catalysts. *J. Hazard Mater.* **2019**, *379*, No. 120773.

(23) López, J.; Reig, M.; Gibert, O.; Cortina, J. L. Integration of Nanofiltration Membranes in Recovery Options of Rare Earth Elements from Acidic Mine Waters. *J. Clean Prod* **2019**, *210*, 1249−1260.

(24) Kegl, T.; Košak, A.; Lobnik, A.; Novak, Z.; Kralj, A. K.; Ban, I. Adsorption of Rare Earth Metals from Wastewater by Nanomaterials: A Review. *J. Hazard Mater.* **2020**, *386*, No. 121632.

(25) Yang, X.; Debeli, D. K.; Shan, G.; Pan, P. Selective Adsorption and High Recovery of La^{3+} Using Graphene Oxide/Poly (N-Isopropyl Acrylamide-Maleic Acid) Cryogel. *Chemical Engineering Journal* **2020**, *379*, No. 122335.

(26) Galhoum, A. A.; Elshehy, E. A.; Tolan, D. A.; El-Nahas, A. M.; Taketsugu, T.; Nishikiori, K.; Akashi, T.; Morshedy, A. S.; Guibal, E. Synthesis of Polyaminophosphonic Acid-Functionalized Poly-(Glycidyl Methacrylate) for the Efficient Sorption of La(III) and Y(III). *Chemical Engineering Journal* **2019**, *375*, No. 121932.

(27) Gao, Y.; Xu, L.; Zhang, M.; Zhang, Q.; Yang, Z.; Yang, J.; Xu, Z.; Lv, Y.; Wang, Y. Ultra-Selective Ion Sieve for Thorium Recovery from Rare Earth Elements Using Oxygen-Rich Microporous Carbon Adsorption. *J. Hazard Mater.* **2021**, *417*, No. 126115.

(28) Awual, M. R.; Hasan, M. M.; Znad, H. Organic−Inorganic Based Nano-Conjugate Adsorbent for Selective Palladium(II) Detection, Separation and Recovery. *Chemical Engineering Journal* **2015**, *259*, 611−619.

(29) Javadian, H.; Ruiz, M.; Saleh, T. A.; Sastre, A. M. Ca-Alginate/Carboxymethyl Chitosan/$Ni_{0.2}Zn_{0.2}Fe_{2.6}O_4$ Magnetic Bionanocomposite: Synthesis, Characterization and Application for Single Adsorption of Nd^{+3}, Tb^{+3}, and Dy^{+3} Rare Earth Elements from Aqueous Media. *J. Mol. Liq.* **2020**, *306*, No. 112760.

(30) Liu, J.; Zeng, L.; Liao, S.; Liao, X.; Liu, J.; Mao, J.; Chen, Y.; Qiu, T.; Ren, S. Highly Efficient Enrichment and Adsorption of Rare Earth Ions (Yttrium(III)) by Recyclable Magnetic Nitrogen Functionalized Mesoporous Expanded Perlite. *Chin. Chem. Lett.* **2020**, *31* (10), 2849−2853.

(31) Jacinto, J.; Henriques, B.; Duarte, A. C.; Vale, C.; Pereira, E. Removal and Recovery of Critical Rare Elements from Contaminated Waters by Living Gracilaria Gracilis. *J. Hazard Mater.* **2018**, *344*, 531−538.

(32) Roosen, J.; Spooren, J.; Binnemans, K. Adsorption Performance of Functionalized Chitosan−Silica Hybrid Materials toward Rare Earths. *J. Mater. Chem. A Mater.* **2014**, *2* (45), 19415−19426.

(33) Borst, A. M.; Smith, M. P.; Finch, A. A.; Estrade, G.; Villanova-de-Benavent, C.; Nason, P.; Marquis, E.; Horsburgh, N. J.; Goodenough, K. M.; Xu, C.; Kynický, J.; Geraki, K. Adsorption of Rare Earth Elements in Regolith-Hosted Clay Deposits. *Nat. Commun.* **2020**, *11* (1), 1−15.

https://doi.org/10.1021/acsnano.4c00691
ACS Nano 2024, 18, 7298−7310

(34) Zhang, Y.; Bian, T.; Jiang, R.; Zhang, Y.; Zheng, X.; Li, Z. Bionic Chitosan-Carbon Imprinted Aerogel for High Selective Recovery of Gd(III) from End-of-Life Rare Earth Productions. *J. Hazard Mater.* **2021**, *407*, No. 124347.
(35) Yang, X.; Debeli, D. K.; Shan, G.; Pan, P. Selective Adsorption and High Recovery of La^{3+} Using Graphene Oxide/Poly (N-Isopropyl Acrylamide-Maleic Acid) Cryogel. *Chemical Engineering Journal* **2020**, *379*, No. 122335.
(36) Srimuk, P.; Su, X.; Yoon, J.; Aurbach, D.; Presser, V. Charge-Transfer Materials for Electrochemical Water Desalination, Ion Separation and the Recovery of Elements. *Nature Reviews Materials* **2020**, *5* (7), 517−538.
(37) Yin, H.; Zhao, S.; Wan, J.; Tang, H.; Chang, L.; He, L.; Zhao, H.; Gao, Y.; Tang, Z. Three-Dimensional Graphene/Metal Oxide Nanoparticle Hybrids for High-Performance Capacitive Deionization of Saline Water. *Adv. Mater.* **2013**, *25* (43), 6270−6276.
(38) Zhang, J.; Fang, J.; Han, J.; Yan, T.; Shi, L.; Zhang, D. N, P, S Co-Doped Hollow Carbon Polyhedra Derived from MOF-Based Core−Shell Nanocomposites for Capacitive Deionization. *J. Mater. Chem. A Mater.* **2018**, *6* (31), 15245−15252.
(39) Mao, M.; Yan, T.; Shen, J.; Zhang, J.; Zhang, D. Selective Capacitive Removal of Heavy Metal Ions from Wastewater over Lewis Base Sites of S-Doped Fe-N-C Cathodes via an Electro-Adsorption Process. *Environ. Sci. Technol.* **2021**, *55* (11), 7665−7673.
(40) Tang, W.; Wang, X.; Zeng, G.; Liang, J.; Li, X.; Xing, W.; He, D.; Tang, L.; Liu, Z. Electro-Assisted Adsorption of Zn(II) on Activated Carbon Cloth in Batch-Flow Mode: Experimental and Theoretical Investigations. *Environ. Sci. Technol.* **2019**, *53* (5), 2670−2678.
(41) Mao, M.; Yan, T.; Shen, J.; Zhang, J.; Zhang, D. Capacitive Removal of Heavy Metal Ions from Wastewater via an Electro-Adsorption and Electro-Reaction Coupling Process. *Environ. Sci. Technol.* **2021**, *55* (5), 3333−3340.
(42) Zhan, W.; Yuan, Y.; Zhang, X.; Liang, Y.; Song, S.; de Jesús Martínez-López, M.; Arauz-Lara, J. L.; Jia, F. Efficient and Selective Lead(II) Removal within a Wide Concentration Range through Chemisorption and Electrosorption Coupling Process via Defective MoS_2 Electrode. *Sep Purif Technol.* **2024**, *329*, No. 125183.
(43) Mao, M.; Yan, T.; Shen, J.; Zhang, J.; Zhang, D. Selective Capacitive Removal of Heavy Metal Ions from Wastewater over Lewis Base Sites of S-Doped Fe-N-C Cathodes via an Electro-Adsorption Process. *Environ. Sci. Technol.* **2021**, *55* (11), 7665−7673.
(44) Zhan, W.; Yuan, Y.; Yang, B.; Jia, F.; Song, S. Construction of MoS_2 Nano-Heterojunction via ZnS Doping for Enhancing in-Situ Photocatalytic Reduction of Gold Thiosulfate Complex. *Chemical Engineering Journal* **2020**, *394*, No. 124866.
(45) Zhan, W.; Jia, F.; Yuan, Y.; Liu, C.; Sun, K.; Yang, B.; Song, S. Controllable Incorporation of Oxygen in MoS_2 for Efficient Adsorption of Hg^{2+} in Aqueous Solutions. *J. Hazard Mater.* **2020**, *384*, No. 121382.
(46) Radisavljevic, B.; Radenovic, A.; Brivio, J.; Giacometti, V.; Kis, A. Single-Layer MoS2transistors. *Nat. Nanotechnol* **2011**, *6* (3), 147−150.
(47) Liu, T.; Shi, S.; Liang, C.; Shen, S.; Cheng, L.; Wang, C.; Song, X.; Goel, S.; Barnhart, T. E.; Cai, W.; Liu, Z. Iron Oxide Decorated MoS_2 Nanosheets with Double PEGylation for Chelator-Free Radiolabeling and Multimodal Imaging Guided Photothermal Therapy. *ACS Nano* **2015**, *9* (1), 950−960.
(48) Ai, K.; Ruan, C.; Shen, M.; Lu, L. MoS_2 Nanosheets with Widened Interlayer Spacing for High-Efficiency Removal of Mercury in Aquatic Systems. *Adv. Funct Mater.* **2016**, *26* (30), 5542−5549.
(49) Pham, V. P.; Yeom, G. Y. Recent Advances in Doping of Molybdenum Disulfide: Industrial Applications and Future Prospects. *Adv. Mater.* **2016**, *28* (41), 9024−9059.
(50) Zou, J.; Cai, Z.; Lai, Y.; Tan, J.; Zhang, R.; Feng, S.; Wang, G.; Lin, J.; Liu, B.; Cheng, H.-M. Doping Concentration Modulation in Vanadium-Doped Monolayer Molybdenum Disulfide for Synaptic Transistors. *ACS Nano* **2021**, *15* (4), 7340−7347.
(51) Yu, X.-Y.; Hu, H.; Wang, Y.; Chen, H.; Lou, X. W. D. Ultrathin MoS_2 Nanosheets Supported on N-Doped Carbon Nanoboxes with Enhanced Lithium Storage and Electrocatalytic Properties. *Angew. Chem., Int. Ed.* **2015**, *54* (25), 7395−7398.
(52) Pierucci, D.; Henck, H.; Ben Aziza, Z.; Naylor, C. H.; Balan, A.; Rault, J. E.; Silly, M. G.; Dappe, Y. J.; Bertran, F.; Le Fèvre, P.; Sirotti, F.; Johnson, A. T. C.; Ouerghi, A. Tunable Doping in Hydrogenated Single Layered Molybdenum Disulfide. *ACS Nano* **2017**, *11* (2), 1755−1761.
(53) Wang, H.; Xiao, X.; Liu, S.; Chiang, C.-L.; Kuai, X.; Peng, C.-K.; Lin, Y.-C.; Meng, X.; Zhao, J.; Choi, J.; Lin, Y.-G.; Lee, J.-M.; Gao, L. Structural and Electronic Optimization of MoS_2 Edges for Hydrogen Evolution. *J. Am. Chem. Soc.* **2019**, *141* (46), 18578−18584.
(54) Deng, S.; Luo, M.; Ai, C.; Zhang, Y.; Liu, B.; Huang, L.; Jiang, Z.; Zhang, Q.; Gu, L.; Lin, S.; Wang, X.; Yu, L.; Wen, J.; Wang, J.; Pan, G.; Xia, X.; Tu, J. Synergistic Doping and Intercalation: Realizing Deep Phase Modulation on MoS_2 Arrays for High-Efficiency Hydrogen Evolution Reaction. *Angew. Chem., Int. Ed.* **2019**, *58* (45), 16289−16296.
(55) Li, S.; Liu, Y.; Zhao, X.; Cui, K.; Shen, Q.; Li, P.; Qu, X.; Jiao, L. Molecular Engineering on MoS_2 Enables Large Interlayers and Unlocked Basal Planes for High-Performance Aqueous Zn-Ion Storage. *Angew. Chem., Int. Ed.* **2021**, *60* (37), 20286−20293.
(56) Sun, B.; Liang, Z.; Qian, Y.; Xu, X.; Han, Y.; Tian, J. Sulfur Vacancy-Rich O-Doped 1T-MoS_2 Nanosheets for Exceptional Photocatalytic Nitrogen Fixation over CdS. *ACS Appl. Mater. Interfaces* **2020**, *12* (6), 7257−7269.
(57) Nan, H.; Wang, Z.; Wang, W.; Liang, Z.; Lu, Y.; Chen, Q.; He, D.; Tan, P.; Miao, F.; Wang, X.; Wang, J.; Ni, Z. Strong Photoluminescence Enhancement of MoS_2 through Defect Engineering and Oxygen Bonding. *ACS Nano* **2014**, *8* (6), 5738−5745.
(58) Zhan, W.; Yuan, Y.; Yao, X.; Yang, B.; Jia, F.; Lin, C.; Arauz-Lara, J. L.; Song, S. Efficient Recovery of Gold(I) from Thiosulfate Solutions through Photocatalytic Reduction with Mn(II)-Doped MoS_2. *ACS Sustain Chem. Eng.* **2021**, *9* (35), 11681−11690.
(59) Ge, J.; Zhang, D.; Jin, J.; Han, X.; Wang, Y.; Zhang, F.; Lei, X. Oxygen Atoms Substituting Sulfur Atoms of MoS_2 to Activate the Basal Plane and Induce the Phase Transition for Boosting Hydrogen Evolution. *Mater. Today Energy* **2021**, *22*, No. 100854.
(60) Tang, J.; Wei, Z.; Wang, Q.; Wang, Y.; Han, B.; Li, X.; Huang, B.; Liao, M.; Liu, J.; Li, N.; Zhao, Y.; Shen, C.; Guo, Y.; Bai, X.; Gao, P.; Yang, W.; Chen, L.; Wu, K.; Yang, R.; Shi, D.; Zhang, G. In Situ Oxygen Doping of Monolayer MoS_2 for Novel Electronics. *Small* **2020**, *16* (42), No. 2004276.
(61) Zhao, Y.; Song, J. G.; Ryu, G. H.; Ko, K. Y.; Woo, W. J.; Kim, Y.; Kim, D.; Lim, J. H.; Lee, S.; Lee, Z.; Park, J.; Kim, H. Low-Temperature Synthesis of 2D MoS_2 on a Plastic Substrate for a Flexible Gas Sensor. *Nanoscale* **2018**, *10* (19), 9338−9345.
(62) Yuan, Y.; Yang, B.; Jia, F.; Song, S. Reduction Mechanism of Au Metal Ions into Au Nanoparticles on Molybdenum Disulfide. *Nanoscale* **2019**, *11* (19), 9488−9497.
(63) Tang, D.; Li, J.; Yang, Z.; Jiang, X.; Huang, L.; Guo, X.; Li, Y.; Zhu, J.; Sun, X. Fabrication and Mechanism Exploration of Oxygen-Incorporated 1T-MoS_2 with High Adsorption Performance on Methylene Blue. *Chemical Engineering Journal* **2022**, *428*, No. 130954.
(64) Zhan, W.; Yuan, Y.; Liu, C.; Chen, P.; Liang, Y.; Wang, Y.; Arauz-Lara, J. L.; Jia, F. Preparation and Application of 0D, 2D and 3D Molybdenite: A Review. *Minerals and Mineral Materials* **2022**, *1* (1), 5.
(65) Liu, J.; Wang, Z.; Li, J.; Cao, L.; Lu, Z.; Zhu, D. Structure Engineering of MoS_2 via Simultaneous Oxygen and Phosphorus Incorporation for Improved Hydrogen Evolution. *Small* **2020**, *16* (4), 1−11.
(66) Xie, J.; Yang, X.; Xie, Y. Defect Engineering in Two-Dimensional Electrocatalysts for Hydrogen Evolution. *Nanoscale* **2020**, *12* (7), 4283−4294.
(67) Hammond, J. L.; Gross, A. J.; Estrela, P.; Iniesta, J.; Green, S. J.; Winlove, C. P.; Winyard, P. G.; Benjamin, N.; Marken, F. Cysteine-

https://doi.org/10.1021/acsnano.4c00691
ACS Nano 2024, 18, 7298−7310

Cystine Redox Cycling in a Gold−Gold Dual-Plate Generator-Collector Microtrench Sensor. *Anal. Chem.* **2014**, *86* (14), 6748−6752.
(68) Yarahmadi, A.; Khani, M. H.; Nasiri Zarandi, M.; amini, Y. Ce(III) and La(III) Ions Adsorption through Amberlite XAD-7 Resin Impregnated via CYANEX-272 Extractant. *Sci. Rep.* **2023**, *13* (1), 1−17.
(69) Kołodyńska, D.; Fila, D.; Hubicki, Z. Static and Dynamic Studies of Lanthanum(III) Ion Adsorption/Desorption from Acidic Solutions Using Chelating Ion Exchangers with Different Functionalities. *Environ. Res.* **2020**, *191*, No. 110171.
(70) Huang, L.; Liu, L.; Huang, W.; Zhao, B.; Shen, Z.; Bao, Y.; Znad, H. Recovery of Lanthanum Cations by Functionalized Magnetic Multi-Walled Carbon Nanotube Bundles. *RSC Adv.* **2021**, *11* (8), 4751−4759.
(71) Kołodyńska, D.; Araucz, K. New Titanium Oxide Sorbent for As(V) and Cr(VI) Removal as Well as La(III) and Nd(III) Recovery. *J. Mol. Liq.* **2020**, *315*, No. 113720.
(72) Awwad, N. S.; Gad, H. M. H.; Ahmad, M. I.; Aly, H. F. Sorption of Lanthanum and Erbium from Aqueous Solution by Activated Carbon Prepared from Rice Husk. *Colloids Surf. B Biointerfaces* **2010**, *81* (2), 593−599.
(73) Ammari Allahyari, S.; Saberi, R.; Sepanloo, K.; Lashkari, A. Adsorptive Separation of La(III) from Aqueous Solution via the Synthesized $[Zn(Bim)_2(Bdc)]_n$ Metal-Organic Framework. *Journal of Rare Earths* **2021**, *39* (6), 742−748.
(74) Song, D.; Park, S.-J.; Kang, H. W.; Park, S. B.; Han, J.-I. Recovery of Lithium(I), Strontium(II), and Lanthanum(III) Using Ca-Alginate Beads. *J. Chem. Eng. Data* **2013**, *58* (9), 2455−2464.
(75) Xu, X.; Zou, J.; Zhao, X. R.; Jiang, X. Y.; Jiao, F. P.; Yu, J. G.; Liu, Q.; Teng, J. Facile Assembly of Three-Dimensional Cylindrical Egg White Embedded Graphene Oxide Composite with Good Reusability for Aqueous Adsorption of Rare Earth Elements. *Colloids Surf. A Physicochem Eng. Asp* **2019**, *570*, 127−140.
(76) Afonso, E. L.; Carvalho, L.; Fateixa, S.; Amorim, C. O.; Amaral, V. S.; Vale, C.; Pereira, E.; Silva, C. M.; Trindade, T.; Lopes, C. B. Can Contaminated Waters or Wastewater Be Alternative Sources for Technology-Critical Elements? The Case of Removal and Recovery of Lanthanides. *J. Hazard Mater.* **2019**, *380*, No. 120845.
(77) Sun, K.; Yao, X.; Yang, B.; Jia, F.; Song, S. Oxygen-Incorporated Molybdenum Disulfide Nanosheets as Electrode for Enhanced Capacitive Deionization. *Desalination* **2020**, *496*, No. 114758.
(78) Shen, P. C.; Lin, Y.; Su, C.; McGahan, C.; Lu, A. Y.; Ji, X.; Wang, X.; Wang, H.; Mao, N.; Guo, Y.; Park, J. H.; Wang, Y.; Tisdale, W.; Li, J.; Ling, X.; Aidala, K. E.; Palacios, T.; Kong, J. Healing of Donor Defect States in Monolayer Molybdenum Disulfide Using Oxygen-Incorporated Chemical Vapour Deposition. *Nature Electronics* **2022**, *5* (1), 28−36.
(79) Xie, J.; Zhang, J.; Li, S.; Grote, F.; Zhang, X.; Zhang, H.; Wang, R.; Lei, Y.; Pan, B.; Xie, Y. Controllable Disorder Engineering in Oxygen-Incorporated MoS_2 Ultrathin Nanosheets for Efficient Hydrogen Evolution. *J. Am. Chem. Soc.* **2013**, *135* (47), 17881−17888.
(80) Jing, Y.; Tan, X.; Zhou, Z.; Shen, P. Tuning Electronic and Optical Properties of MoS_2 Monolayer via Molecular Charge Transfer. *J. Mater. Chem. A* **2014**, *2* (40), 16892−16897.
(81) Wu, Y.; Xu, Q.; Huang, L.; Huang, B.; Hu, P.; Xiao, F.; Li, N. Encapsulation of Sulfur in MoS_2-Modified Metal-Organic Framework-Derived N, O-Codoped Carbon Host for Sodium−Sulfur Batteries. *J. Colloid Interface Sci.* **2024**, *654*, 649−659.
(82) Yang, S.; Jiang, Q.; Zhang, K. Few-Layers 2D O−MoS_2 TFN Nanofiltration Membranes for Future Desalination. *J. Membr. Sci.* **2020**, *604*, No. 118052.

https://doi.org/10.1021/acsnano.4c00691
ACS Nano 2024, 18, 7298−7310